J Solid State Electrochem (2014) 18:1319–1334
DOI 10.1007/s10008-013-2233-x

ORIGINAL PAPER

Kinetics and mechanism of oxygen electroreduction on Vulcan XC72R carbon black modified by pyrolysis products of cobalt 5,10,15,20-tetrakis(4-methoxyphenyl)porphyrine in a broad pH interval

Galina V. Zhutaeva · Vera A. Bogdanovskaya · Elena S. Davydova · Leonid P. Kazanskii · Michail R. Tarasevich

Received: 5 June 2013 / Revised: 13 August 2013 / Accepted: 16 August 2013 / Published online: 27 September 2013

Abstract The kinetic parameters of oxygen reduction reaction on Vulcan XC72R carbon black, carbon black modified by pyrolysis products of cobalt 5,10,15,20-tetrakis(4-methoxyphenyl)porphyrine named by MXC72R, and commercial Pt/C platinum catalyst have been considered. Comparison of their electrochemical properties including pH influence in a broad interval from 0.3 to 14.6 has shown platinum-similar behavior of MXC72R in the reaction under study. An increasing order of electrochemical activity for oxygen reduction reaction is obtained, namely XC72R<MXC72R<Pt/C. The mechanism of oxygen reduction reaction is discussed emphasizing the important accelerating role of protonation of adsorbed oxygen molecule and inhibiting role of oxygen-containing species (formed due to water molecule discharge) and strongly adsorbed foreign species. The importance of the research on oxygen reduction reaction in a broad pH interval to evaluate the efficiency of various precious metal-free catalytic systems in comparison to platinum is emphasized.

Keywords Oxygen reduction reaction · Turbostratic carbon · Platinum · Porphyrin · Protonation

Introduction

Professor Vladimir S. Bagotsky put the investigations in the field of oxygen electroreduction reaction in place of one of the top priority electrochemical tasks [1, 2]. His works on oxygen electroreduction on mercury [3] are considered as classical. Prof. V. Bagotsky and co-workers made the major theoretical and practical contribution to the development of the theory of rotating ring disk electrode [4–6] permitting to calculate rate constants of individual stages of the oxygen electroreduction multiple-stage process. Prof. V. Bagotsky and co-workers actively supported the research on developing oxygen catalysts based on metal chelates [7].

Vulcan XC72R (hereafter referred to as XC72R) carbon black, which can be classified as turbostratic carbon [8], is the most widespread commercial carbon support for the preparation of platinum and nonplatinum cathodic catalysts for low-temperature proton exchange membrane fuel cell. Being one of the best characterized carbon materials, XC72R was chosen as the catalyst support discussed in the present paper. The intrinsic properties of a number of carbon materials in oxygen reduction reaction (ORR) and the properties for multiwalled carbon nanotubes (MWCNT) in a broad pH interval were studied in detail by Kruusenberg et al. [9, 10]. Authors attributed the pH dependence of the ORR activity for MWCNT in alkaline solutions to electrocatalysis by surface quinone groups [11].

At present, the most popular direction of nonplatinum cathodic catalysts development is the creation of nitrogen-containing structures on high-disperse carbon supports. The cathodic catalyst was synthesized for the first time by pyrolysis of cobalt dibenzotetraazaannulene in temperature intervals of 600–1,000 °C [12]. The enhancement of electrocatalytic activity of a variety of N_4 complexes subjected to heat treatment at 400–500 °C in the ORR was shown in [13]. In [7], independently, the synthesis of cathodic catalysts by pyrolysis of porphyrines and phthalocyanines of different metals at

G. V. Zhutaeva (✉) · V. A. Bogdanovskaya · E. S. Davydova · L. P. Kazanskii · M. R. Tarasevich
Frumkin Institute of Physical Chemistry and Electrochemistry, Russian Academy of Sciences, Leninsky prospect, 31, 119071 Moscow, Russia
e-mail: zh@elchem.ac.ru

800–900 °C was described. The high stability of air cathodes on the basis of these catalysts in sulfuric acid electrolyte during 10,000 h was shown.

The highest electrocatalytic activity in the ORR was obtained for pyrolyzed cobalt 5,10,15,20-tetrakis(4-methoxyphenyl)porphyrine (CoTMPP). This N_4 complex was used as the precursor in works of several research groups [14–26]. Thus, CoTMPP pyrolysis procedures are well-documented and electrochemical properties of catalysts on the basis of CoTMPP are rather well-characterized. This allows us to consider this system as a "model" one (or typical representative of nonplatinum cathodic catalysts group) and use it as a "reference" nonplatinum catalyst. The catalyst synthesized on the basis of XC72R modified by CoTMPP pyrolysis products in the present paper is referred to as MXC72R.

In spite of the significant amount of investigations partially generalized in [27–29], up to now the structure of active center (AC) of catalyst synthesized with CoTMPP is the question under discussion. Especially, this concerns the role of metal (in this case, cobalt) in formation of nitrogen-containing AC. According to [29–31], the role of cobalt in the composition of AC comes down to oxygen molecule activation. In the investigations of Popov's group [32, 33], AC is thought to be composed of nitrogen atoms in quaternary and pyridine forms and cobalt atoms are believed to influence only the ligand pyrolysis process. The role of nitrogen doping in the change of some physical properties and electrocatalytic behavior in the molecular ORR of carbon nanotubes was studied in detail in the works of Stevenson et al. [34–37] and of Kruusenberg et al. [38] for CoTMPP pyrolyzed on functionalized MWCNT.

This work is a comparative study on kinetics and mechanism of the ORR on XC72R and MXC72R in broad pH interval (0.3–14.6). Earlier, such investigations were performed only on nonpyrolyzed N_4 complexes (phthalocyanines, porphyrins, including CoTMPP) adsorbed on carbon support [39]. Also, measurements were taken on catalyst 40 wt% Pt HiSPEC 4000 (40Pt/C) to compare with the data obtained on XC72R and MXC72R. In this work, well-known catalytic systems were used and the problem of achieving of high specific parameters was not faced by us. Here, the experimental conditions ensuring the proceeding of electrochemical processes on XC72R and MXC72R in kinetic mode were selected.

Experimental

Catalytic materials

Vulcan XC72R carbon black was not subjected to any preliminary treatment before carrying out the investigation or its modification with CoTMPP. As was shown in [19], the optimal activity of the catalyst is achieved when three monolayers of CoTMPP per unit of real surface area of carbon support is used. In the case of XC72R, CoTMPP amount is equal to 30 wt%. For catalyst synthesis, CoTMPP dispersion in chloroform was admixed with XC72R carbon black suspension in ethanol subjected to ultrasonic treatment for 1 h and dispersed together for 2 h. Then, the solvent was removed by evaporation on water bath and the residual was pyrolyzed at 850 °C in argon atmosphere.

With the aim of the removing soluble pyrolysis products, treatment in 0.5 M H_2SO_4 in 2 h at 60 °C with air bubbling was used; subsequent catalyst washing with bidistilled water to neutral reaction was used. It is a standard practice for catalysts preparation after high-temperature synthesis to the investigations of the ORR.

For the study of the surfaces of XC72R and catalysts before and after their pyrolysis, X-ray photoelectron spectrometry (XPS) was used. There is no nitrogen in the initial carbon support and the oxygen content does not exceed 1 at.% (Fig. 1a). Figure 1 shows XPS for (a) XC72R, (b) CoTMPP pyrolyzed without carbon support, and (c) MXC72R. In all the cases, peaks corresponding to cobalt, oxygen, nitrogen, and carbon are present in the survey spectra. Table 1 represents (XC72R+CoTMPP) and MXC72R surface composition.

Atomic relationship between cobalt and nitrogen in initial nonpyrolyzed porphyrin is close to the formal composition of porphyrin, N/Co=4. Pyrolysis of porphyrins results in noticeable change in spectra. Pyrolysis of porphyrin at 850 °C results in practically complete destruction with the removal of the carbon part. It should be noted that data in Table 1 show a relative surface composition (at a depth of about 10 nm) of the initial system and pyrolysis products which represent an absolutely new system of carbon modified by nitrogen. The analysis of XPS C1s energy region is not simple due to several states of carbon on the surface. However, it is considered that the main carbon peak-binding energy is equal to 284.3 eV (Fig. 2a). This results in Co $2p_{3/2}$ peak-binding energy equal to 780.3 eV (Fig. 2d), which can be due to Co–N and cobalt oxides bonding [40]. This conclusion follows not only from insignificant surface content decrease of nitrogen in relation to cobalt but also to the appearance of oxygen peak at 530.4 eV corresponding to cobalt oxides. As the result of pyrolysis, three states of nitrogen are discovered. Asymmetric shape of nitrogen XPS in catalyst on carbon black assumes the existence of several states of nitrogen which are characterized by three peaks at 402.0, 400.3, and 398.5 eV as a result of spectrum factorization. The first peak can be related to graphite (quaternary) nitrogen atom. The second and third ones can be due to pyrrole and pyridine nitrogen atoms which can participate in the binding with cobalt [32].

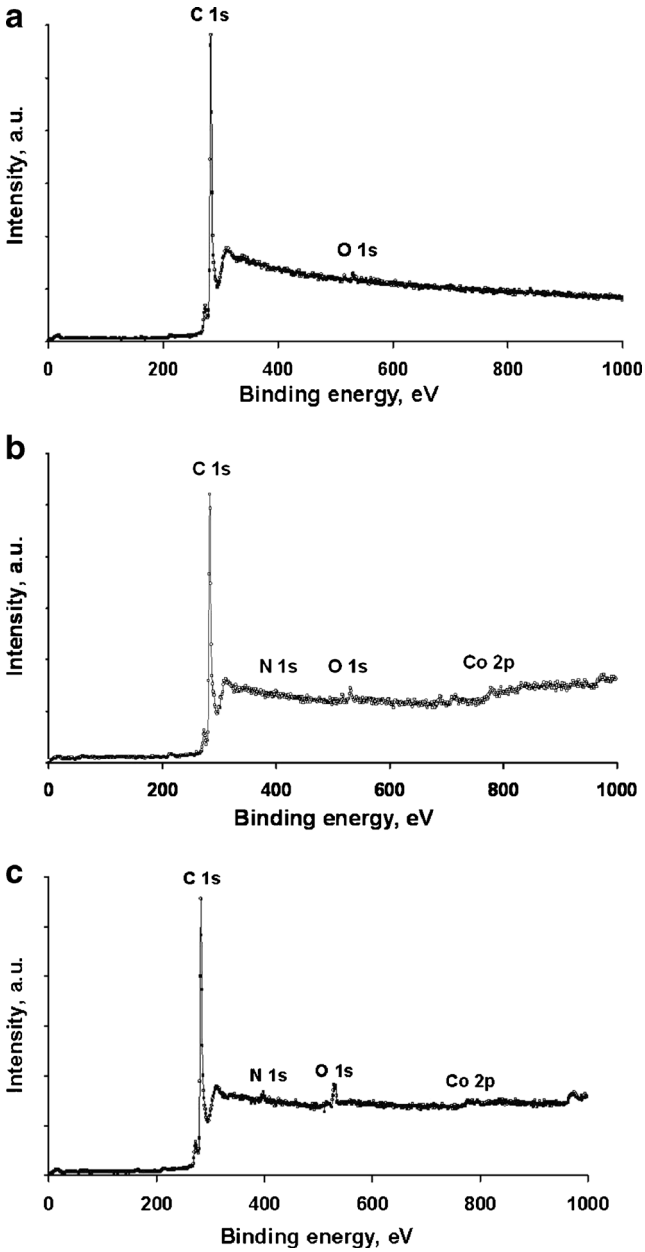

Fig. 1 XPS for XC72R (**a**), CoTMPP pyrolyzed without carbon support (**b**) and MXC72R (**c**)

Thus, the catalyst synthesis on XC72R results in porphyrin destruction and removal of the nitrogen part; nevertheless, nitrogen remained in the specimen and fixed on definite positions in carbon black structure which was kept during the synthesis. The results of structural and corrosion studies of MXC72R are described in detail in [41].

Table 1 Atomic content of catalyst components: initial (XC72R+CoTMPP) and pyrolysis products of CoTMPP on XC72R

Atom	C1s	O1s	N1s	Co2p
Atom.%, (XC72R+CoTMPP) before pyrolysis	95.9	2.4	1.34	0.36
Atom.%, pyrolysis products	94.2	2.6	2.5	0.7

Rotating disk electrode method

The measurements of kinetic parameters of catalytic systems and their mass charge density (MCD) were performed on glassy carbon disk electrode (S=0.196cm^2) with thin layer of catalyst. The catalyst was applied on the electrode from the catalytic ink which is a suspension of 2 mg catalyst in 300 μl ethanol and 200 μl of 0.05 % Nafion. The mixture was dispersed in an ultrasound bath for 15 min and an aliquot was applied on the electrode. The electrode was dried for 30 min. Electrochemical parameters of commercial platinum catalyst (40 wt% Pt HiSPEC 4000) were measured as recommended in [42, 43] at catalyst loading ca. 14 μg Pt cm^{-2}. Studies of the electrochemical properties of XC72R and MXC72R were performed for wide range of loadings (0.02–1.0 mg cm^{-2}) as recommended in [44].

Polarization curves of the ORR were measured at potential scan rates of 0.002 and 0.005 V s^{-1} at 25 °C unless otherwise specified. The measurements of cyclic voltamograms (CVA) were performed in electrolyte under argon atmosphere at a potential scan rate of 0.1 V/s. The values of MCD for XC72R and MXC72R were calculated by integration of the CVA in the potential range of 0–1.2 V normalized per mass unit.

The mass transport-corrected Tafel plots were obtained by extrapolation of experimental data in $\frac{1}{i} = \mathrm{f}\left(\omega^{-1/2}\right)$ coordinates to the infinite rotation rate. For the first time, this method of "reverse extrapolation" was proposed by Frumkin et. al. [45, 46] for determination of kinetic current values of molecular hydrogen and chlorine oxidation reactions and thereafter proved theoretically by Levich and Koutezkii [47] by an the equation:

$$\frac{1}{i} = \frac{1}{i_\mathrm{k}} + \frac{1}{i_\mathrm{L}} = \frac{1}{i_\mathrm{k}} + \frac{1}{0.62nFD^{2/3}\nu^{-1/6}\omega^{1/2}} \quad (1)$$

where i_k is the kinetic current density of the ORR, i_L is the limiting diffusion current density, n is the electron number participating in the reduction reaction of one oxygen molecule, F is the Faraday constant, D is the oxygen diffusion coefficient, c is the oxygen concentration in solution bulk, ν is the kinematic viscosity, and ω is the angular rotation rate.

From Eq. 1, it is seen that for the data obtained at a constant temperature in the same solution $\frac{1}{i} = \mathrm{f}\left(\omega^{-1/2}\right)$ dependence is linear and at $\frac{1}{\omega^{\frac{1}{2}}} \to 0 \frac{1}{i} = \frac{1}{i_\mathrm{k}}$. So, maximal value of kinetic current density can be determined extrapolating experimental data to infinite rotation rate.

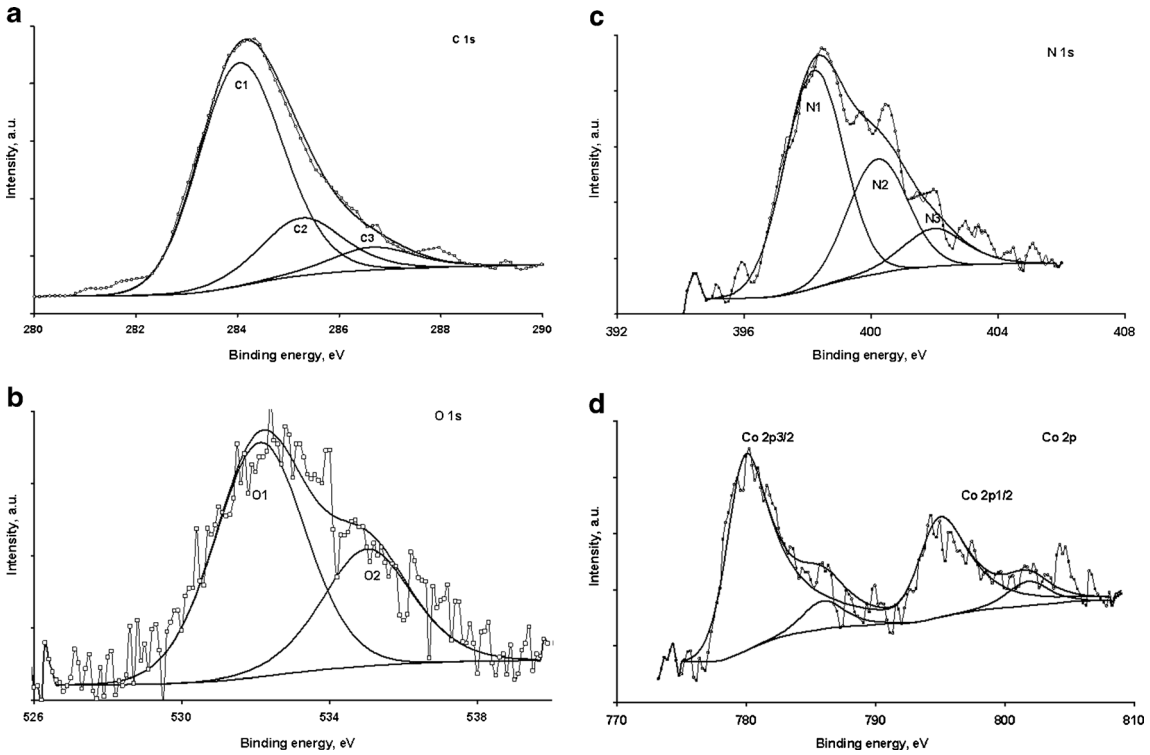

Fig. 2 XPS for MXC72R for individual elements: C1s (**a**), O1s (**b**), N1s (**c**), Co2p (**d**)

The reproducibility and precision of obtained values of the electrochemical parameters depend on three factors. These are (1) batch-to-batch reproducibility of MXC72R synthesized in the laboratory, (2) the reproducibility of catalyst loading applied on the electrode, and (3) the precision of the electrochemical measurements. The latter, in its turn, depends on the equipment used. In this work, no less than three independent tests were taken to eliminate random errors. The average relative error of electrochemical parameters such as mass charge density and electrocatalytic mass activity does not exceed ±15 %.

Electrochemical measurements were performed in electrolytes pH which are in the interval of 0.3–14.6. The sulfuric acid solutions were prepared from 18 M H_2SO_4 (Sigma-Aldrich Co.). For preparation of neutral solutions and for correction of pH and ionic strength, the following reactants were used: K_2SO_4 (Reakhim, Russia), Na_2HPO_4 (Panreac), KH_2PO_4 (Panreac), KCl (Reakhim, Russia), and NaOH (Merck). Alkaline solutions were prepared from KOH (Merck). Mercury–mercury sulfate (Hg/Hg_2SO_4) electrode served as reference electrode for 0.5 M H_2SO_4 solutions; for 4 M KOH solutions, mercury–mercury oxide electrode (Hg/HgO) was used. For solutions with pH from 2.2 to 13.0, the values of the reference electrode potentials were determined in experiments against reversible hydrogen electrode using salt bridges. All the potentials were converted so as to refer to the standard hydrogen electrode (SHE).

Rotating ring disk electrode method

The study by rotating ring disk electrode (RRDE) method was performed in 0.1 M H_2SO_4 and KOH solutions at 25 °C. The diameter of glassy carbon disk is equal to 5.0 mm; external and inner diameters of platinum ring are equal to 7.5 and 6.5 mm, respectively.

Calculated value of collection efficiency N [48] for a given geometry of RRDE equals 0.21±0.01. Platinum ring electrode was platinized to achieve roughness factor ca. 80–100 [49]. Then, it was periodically subjected to electrochemical activation (in background solution) by cycling its potential in the interval of 0.05–1.40 V for the achievement of diffusion-limiting current values of hydrogen peroxide electrooxidation (at 10^{-3} M H_2O_2 in background solution) in the potential interval of 1.1–1.25 V. At measurements with RRDE, the ring potential was maintained at the value of 1.23 V.

For experimental evaluation of N value, $\left[Fe(CN)_6\right]^{4^-/3^-}$ system in 0.1 M KOH was used. The ring potential was maintained at 0.55 V. Within the limits of experimental error ±5 %, N value composed 0.206 and 0.187 for electrodes with catalyst loading of 0.15 and 0.8 mg cm^{-2}, respectively, and does not depend on electrode rotation rate in the interval of 500–1,500 rpm. These data correspond to the results in [50]. The measurements were performed with the use of Pine Instrument at potential sweep rate of 0.005 V s^{-1} and electrode rotation rate of 500–2,000 rpm.

Mechanistic interpretation of oxygen reduction data on a RRDE was performed according to the simplified ORR scheme [5]:

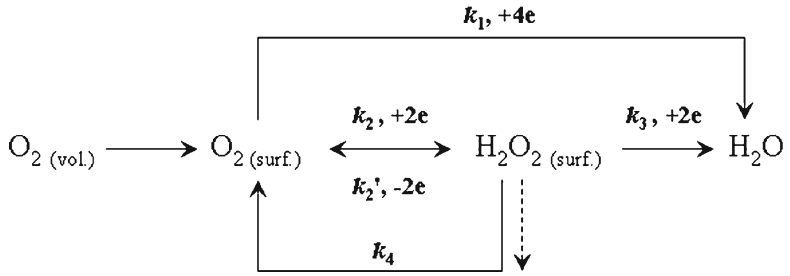

where k_1 is the rate constant of oxygen electroreduction reaction to H_2O

k_2 is the rate constant of oxygen electroreduction reaction to H_2O_2

k_3 is the rate constant of H_2O_2 electroreduction reaction to H_2O

k_4 is the rate constant of H_2O_2 catalytic decomposition

k_2' is the rate constant of H_2O_2 electrooxidation reaction

The schemes which include hydrogen peroxide adsorption are also known [51, 52]. Wroblowa's method uses a new approach permitted to determine adsorption rate of hydrogen peroxide and suitable only for flat electrodes. Here, we use the simplified ORR scheme [5].

The H_2O_2 yield was calculated according to [53] with the formula

$$H_2O_2 = \frac{2I_R/N}{I_D + I_R/N} \times 100\% \quad (2)$$

For calculation of values of the rate constants of individual stages, the following equations were used:

$$\frac{I_D \times N}{I_R^d} = 1 + 2\frac{k_1}{k_2} + \frac{1}{z_{H_2O_2}}\left[k_3 + (k_3 + k_4) \times \left(1 + 2\frac{k_1}{k_2}\right)\right] \times \omega^{-1/2} \quad (3)$$

$$\frac{(I_D^d - I_D) \times N}{I_R^d} = 1 + 2\left(\frac{D_{O_2}}{D_{H_2O_2}}\right)^{2/3} \times \frac{k_3 + k_4}{k_2} + 2\frac{z_{O_2}}{k_2}\omega^{1/2} \quad (4)$$

The graphical processing was performed in $\frac{(I_D^d - I_D) \times N}{I_R^d}, \omega^{1/2}$ and $\frac{I_D \times N}{I_R^d}, \omega^{-1/2}$ coordinates where $I_D{}^d, I_D$, are values of limiting diffusion and experimental current on rotating disk electrode (RDE), respectively; $I_R{}^d$ is the current value on ring electrode; N is collection efficiency; $z_{H_2O_2}$ и z_{O_2} are transport parameters for H_2O_2 and O_2, respectively. For calculation, the following data were used. For $0.1\,M\,H_2SO_4\,C_{O_2} = 1.12 \times 10^{-6} mol\,cm^{-3}$ [54]; $D_{O_2} = 1.8 \times 10^{-5} cm^2 s^{-1}$ [54]; $D_{H_2O_2} = 1.45 \times 10^{-5} cm^2 s^{-1}$ [55]; $\nu = 1.07 \times 10^{-2} cm^2 s^{-1}$ [56]. For $0.1M\,KOH: C_{O_2} = 1.2 \times 10^{-6} mol\,cm^{-3}$ [57], $D_{O_s} = 1.9 \times 10^{-5} cm^2 s^{-1}$ [57]; $\nu = 0.905 \times 10^{-2} cm^2 s^{-1}$ [57], $D_{H_2O_2} = 0.93 \times 10^{-5} cm^2 s^{-1}$ [58].

Taking measurements in a broad pH value interval is an important methodology for studying multi-electron transfer reactions. In [59], numerous works on ORR kinetics were generalized. The considerable informativity of investigations in a broad interval of pH values for the establishment of the ORR mechanism was illustrated in works [11, 39, 60–62] at polycrystalline platinum [60], at (100) gold plane [61], at multiwalled carbon nanotubes [11], and at initial nonpyrolyzed adsorbed CoTMPP [39, 62]. This approach was also used to study the superoxide role of ORR in glassy carbon [63], in platinum in weak alkaline solutions [64], and in investigation of the same reaction at nitrogen-containing carbon materials in neutral and alkaline solutions [65]. Spectroscopic identification of intermediates of the ORR at gold in alkaline and acid solutions [66] confirmed the four-electron serial pathway in alkaline medium at active surfaces such as Au(100).

Results and their discussion

The focus of this work is on the influence of electrolyte pH value on electrocatalytic activity and selectivity of XC72R and MXC72R in the proceeding ORR in the kinetic regime. The data would allow us to make conclusions on the ORR pathways and mechanism.

Electrochemical parameters of XC72R and MXC72R at various loadings

The optimal catalyst loading was chosen to ensure the kinetic regime of the proceeding ORR via the formation of uniform

equally accessible catalytic layer. Figure 3 shows the polarization curves for the ORR on the electrodes with various XC72R loadings in 1 M KOH. As seen, the enhancement of carbon black amount on the electrode does not practically influence the limiting current value of the first wave related to the formation of HO_2^-. This fact speaks about the stability of HO_2^- intermediate product as on the surface and in the bulk of the active layer. Considerable increase of the ORR current at the potentials of the second wave with the increase of XC72R amount indicates the growing of HO_2^- electrochemical reduction rate.

Figure 4 represents polarization curves for the ORR in (a) 0.5 M H_2SO_4 and (b) 1 M KOH on the electrodes with various loadings of MXC72R catalyst. In studied interval of catalyst loadings (m, milligram per square centimeter), the shift of half-wave potential ($E_{1/2}$) into anodic side and the growth of the limiting current values are observed in both electrolytes. In the case of 1 M KOH, limiting current value at 0.4 mg cm^{-2} exceeds insignificantly the theoretical value of diffusion current for four-electron reaction. In contrast, in the case of carbon black (Fig. 3), the shift of the polarization curves with the increase of catalyst loadings is observed only for the second wave corresponding to HO_2^- reduction to OH^-.

Apparently, these phenomena, to a great extent, are due to the deepening the ORR process at the expense of electrocatalytic decomposition of intermediate product in three-dimensional porous layer and as a result more complete O_2 electroreduction. Such an explanation has been earlier proposed by authors [44, 67–70] investigating the influence of catalytic layer thickness on hydrogen peroxide yield in acid solution. In [67, 68], the growth of the selectivity of the ORR to water at enhancement of catalyst amount per surface unit was observed for platinum catalysts synthesized on supports.

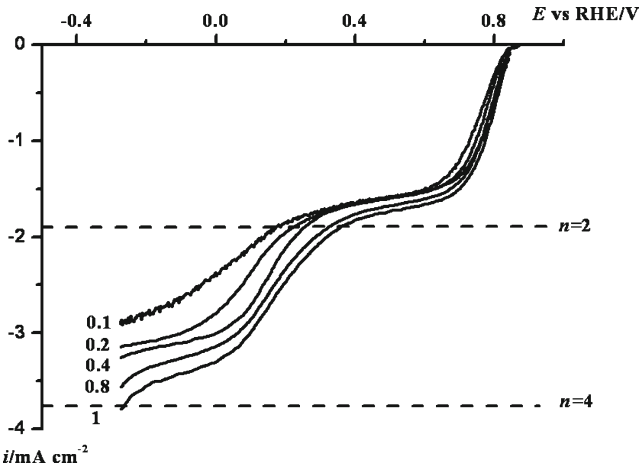

Fig. 3 Polarization curves for the ORR at XC72R various loadings on RDE. 1 M KOH, 60 °C, 1,500 rpm, 0.005 V s^{-1}. *Numbers near the curves* indicate XC72R loading on RDE, in milligram per square centimeter. *Dashed lines* show limiting diffusion current density values for $n=2$ and $n=4$

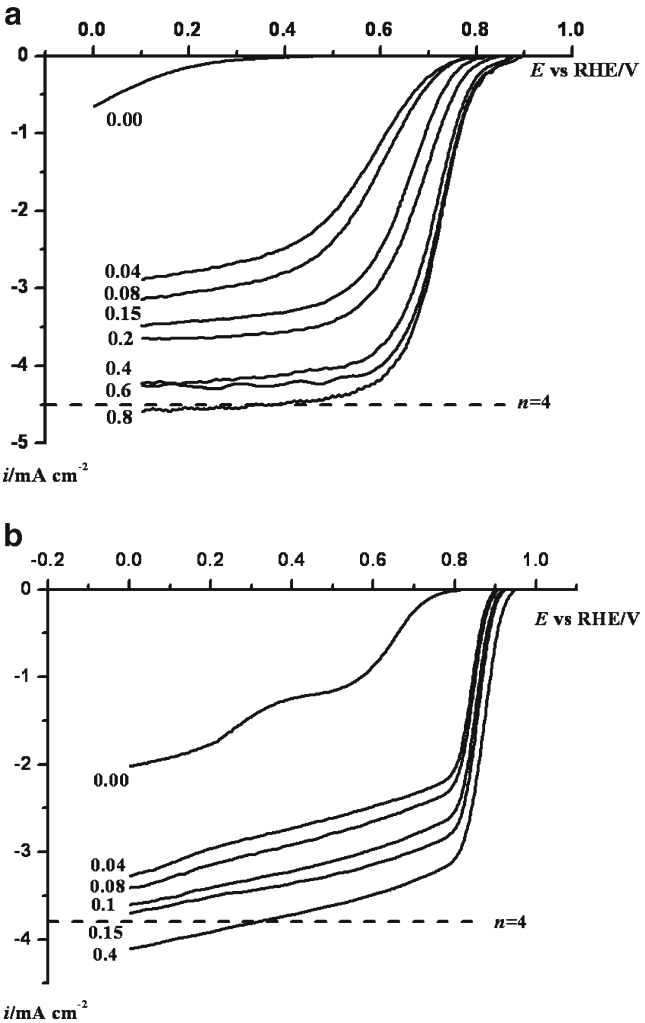

Fig. 4 Polarization curves for the ORR at MXC72R various loadings on RDE. 0.5 M H_2SO_4 (**a**), 1 M KOH (**b**), 60 °C, 1,500 rpm, 0.005 V s^{-1}. *Numbers near the curves* indicate MXC72R loading on RDE, in milligram per square centimeter. *Dashed lines* show limiting diffusion current density values for $n=4$. *Curve* with 0.00 corresponds to XC72R carbon black

The authors [44, 69, 70] show that the above-indicated dependence takes place also for the low-active catalysts. Based on the requirements of hydrogen peroxide minimal yield, in [67] "optimal" amounts of Pt in Pt/C and Pt/NSTF catalysts were determined as 0.015 and 0.04 mg cm^{-2} and for Se/Ru/C and Fe-N-C systems "optimal" catalyst loadings as 0.1 and 0.8 mg cm^{-2}, respectively.

Figure 5a shows the polarization curves of oxygen reduction on disk electrode at the MXC72R loadings 0.15, 0.2, and 0.4 mg cm^{-2} and the corresponding hydrogen peroxide oxidation curves on ring electrode. As shown in special experiments, the collection efficiency N depends insignificantly on catalyst loading [71]. In the kinetic region ($E \geq 0.7$ V), the enhancement of I_D and I_R values are observed with the increase of catalyst loading due to the growth of AC number per unit electrode geometric surface. In the diffusion region

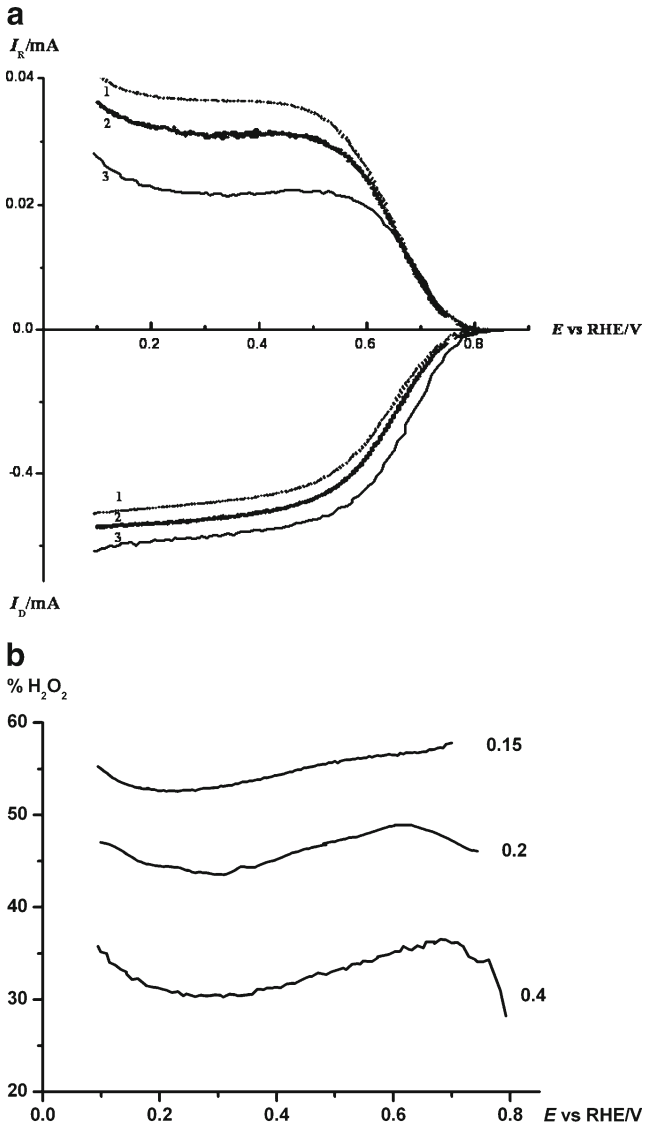

Fig. 5 Polarization curves for the ORR on a thin-film RRDE with MXC72R and simultaneously recorded ring currents for a ring potential of E_R=1.23 V at MXC72R loading at RDE of in milligram per square centimeter: 0.15 (*1*), 0.2 (*2*), and 0.4 (*3*) (**a**), and potential influence on the H_2O_2 yield at the different catalyst loading. *Numbers near the curves* indicate MXC72R loading on RDE, in milligram per square meter (**b**). 0.1 M H_2SO_4, 25 °C, 500 rpm

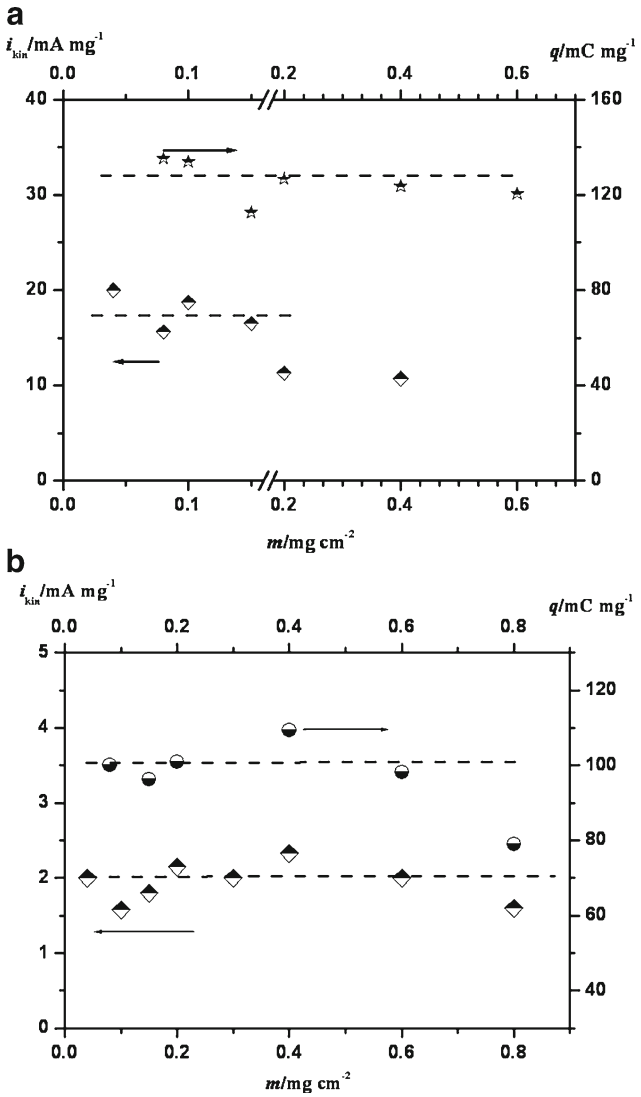

Fig. 6 Dependence of mass charge density and mass activity for the ORR on MXC72R catalyst mass at RDE in 1 M KOH at E=0.85 V (**a**) and 0.5 M H_2SO_4 at E=0.75 V (**b**). The measurement activity conditions are the same as Fig. 4

(E<0.5 V), a sharp decrease of H_2O_2 oxidation current at ring electrode is observed at enhancement of catalyst loading. Calculations made using Eqs. (3) and (4) at E=0.5 V showed that the constant sum (k_3+k_4) characterizing H_2O_2 transformation is increased from 1.5×10^{-3} to 4.3×10^{-3} cm s^{-1} at enhancement of catalyst content from 0.15 to 0.8 mg cm^{-2}. Herewith, the yield of H_2O_2 was calculated according to [53] with formula (2) is declining from 56 to 29 % (Fig. 5b).

Figure 6a,b show $q=f(m)$ and $i_{kin}=f(m)$ dependency diagrams. The dependency of the mass charge density (q, millicoulomb per milligram) on the catalyst loading characterizes the electrochemical accessibility of the inner catalyst surface to electrolyte ions. The dependency of the mass activity (i_{kin}, milli-Ampere per milligram) on the amount of the catalyst, in turn, characterizes the accessibility of the inner catalyst surface to the electroactive substance molecules, namely, oxygen molecules. The values of the catalytic activity are represented as E=0.75 V for 0.5 M H_2SO_4 and E=0.85 V for 1 M KOH. From the data presented, it is evident that in alkaline electrolyte, the kinetic regime of the ORR is ensured in much more narrow range of catalyst loadings (<0.2 mg cm^{-2}) in contrast to acid solution (<0.6 mg cm^{-2}). It is mainly due to higher (approximately in order of magnitude) value of mass activity in 1 M KOH. In alkaline solutions, the decrease of overvoltage of the slow stage of the ORR, namely, the first electron transfer to oxygen molecule towards as two- and four-electron reactions [72] begins to play a considerable role as a result of the lowering of oxygen adsorption energy. The last

effect results in decrease of reaction selectivity to water. In alkaline solution, a single polarization wave for MXC72R is formed with the half wave potential close to platinum. The decrease of reaction overvoltage in alkaline solutions enhances a competitive ability of nonplatinum materials. As in the case of platinum, at analysis of experimental data, three basic factors should be appreciated, namely, thermodynamic of oxygen reaction, the value of oxygen adsorption energy, and the possibility of participation of proton in slow stage. This problem was discussed in more detail in [73].

Thus, the optimal catalyst loading was chosen to be 0.15 mg cm^{-2} for both electrolytes. The evaluation shows the thickness of such a layer to be less than 15–20 % higher than the thickness of active layers of the most widely used platinum catalysts [42, 43] because of different densities of both catalytic systems under consideration. Moreover, further enhancement of catalyst loading does not result in substantial changing of $E_{1/2}$ potential.

As the object of the present work is the investigation of the ORR pathway and its mechanism in a broad pH interval, the main experimental data discussed were obtained at a material loading of 0.1 mg cm^{-2} for carbon black XC72R and 0.15 mg cm^{-2} for MXC72R. The interval of 0.1–0.15 mg cm^{-2} was used for XC72R carbon black and MXC72R in all the solutions for the sake of maintenance of invariability of layer thickness (the densities of XC72R and MXC72R are near 0.4 g cm^{-3}).

pH effect on XC72R and MXC72R characteristics

In [39, 59–63], as for example, the significant informativity of investigations in a broad pH interval has been shown in terms of establishment of the ORR mechanism.

This approach was used in [63] to study the superoxide ion role on oxygen electroreduction in glassy carbon. The data were obtained in conditions of nonstationary measurements and it is difficult to use them for analysis of the ORR kinetics and mechanism at its stationary proceeding.

In the present work, the study of the pH value solution influence on the ORR electrochemical parameters for XC72R and MXC72R systems permitted to obtain necessary data about selectivity, electrochemical activity, and also pathways and mechanism of reactions. The data illustrating pH effect on the ORR are represented in Table 2 and Figs. 7, 8, 9, and 10.

Mass charge density

As in acid and alkaline solutions, about twofold enhancement (Table 2) of MCD is observed in potential interval of $\Delta E = 0$–1.2 V for MXC72R in comparison with XC72R. We suppose that this is due to the formation of nitrogen-enriched carbon phase during the pyrolysis process and, as a result, of new AC on carbon support surface. CVA for XC72R in acid and neutral solutions (for MXC72R in acid solutions only) are characterized by reversible redox processes of oxygenated surface groups (the so called quinone–hydroquinone transition) [8].

Table 2 Electrochemical parameters of XC72R (0.1 mg cm^{-2}) and MXC72R. (0.15 mg cm^{-2}) 0.002 V s^{-1}, 635 rpm

pH	E_s, V	$E_{1/2}$, V	n[a]	q, mC mg^{-1}
XC72R[b]				
0.3	0.700	0.138	1.93	56
7.0	0.432	0.076	1.94	33
13	0.163	0.063	1.92	32
14	0.102	0.036	1.88	61
MXC72R				
0.3	0.857	0.710	3.06	121
7.0	0.343	0.232	3.10	80
13	0.232 (0.224)[c]	0.110 (0.106)[c]	3.41	88
14	0.190	0.076	3.18	107

[a] Electron number at limiting current potential

[b] In the case of XC72R, $E_{1/2}$ values correspond to the first wave potentials

[c] E and $E_{1/2}$ values in brackets were measured in solutions with K_2SO_4 additive

For both XC72R and MXC72R, the decrease of MCD takes place at pH changing from 0.3 to 7.0 and, conversely, the increase of MCD is observed when changing the pH from neutral to alkaline. The first effect could be explained by lowering the charge in the range of quinone–hydroquinone transition and the second one could be referred to the enhancement of OH^- ion adsorption. It agrees with the data in [74, 75]. In [50], nitrogen-modified carbon nanotubes were studied and the authors deduced that boundary structure defects and broken links of nitrogen-doped materials are responsible for MCD increase.

pH effect on polarization curves

In solutions with pH of 0.3 and 2.2, the only bend on the curve is observed for XC72R (Fig. 8) corresponding to the transfer of two electrons (Table 2) and electroreduction of O_2 to H_2O_2. The wave of H_2O_2 reduction apparently overlaps with hydrogen evolution. When passing to the sub-acid, neutral, and alkaline solutions, two polarization waves are observed. The wave at the more negative potentials is accounted for by hydrogen peroxide reduction to water (or OH^- in alkaline solutions).

Disregarding the pH value, polarization curves on MXC72R catalyst have a single limiting diffusion current wave (Fig. 9) in contrast to carbon black. As it will be proved below, this is due to the simultaneous proceeding of the ORR via two- and four-electron ways with the formation of water and hydrogen peroxide as an undesirable by-product. This

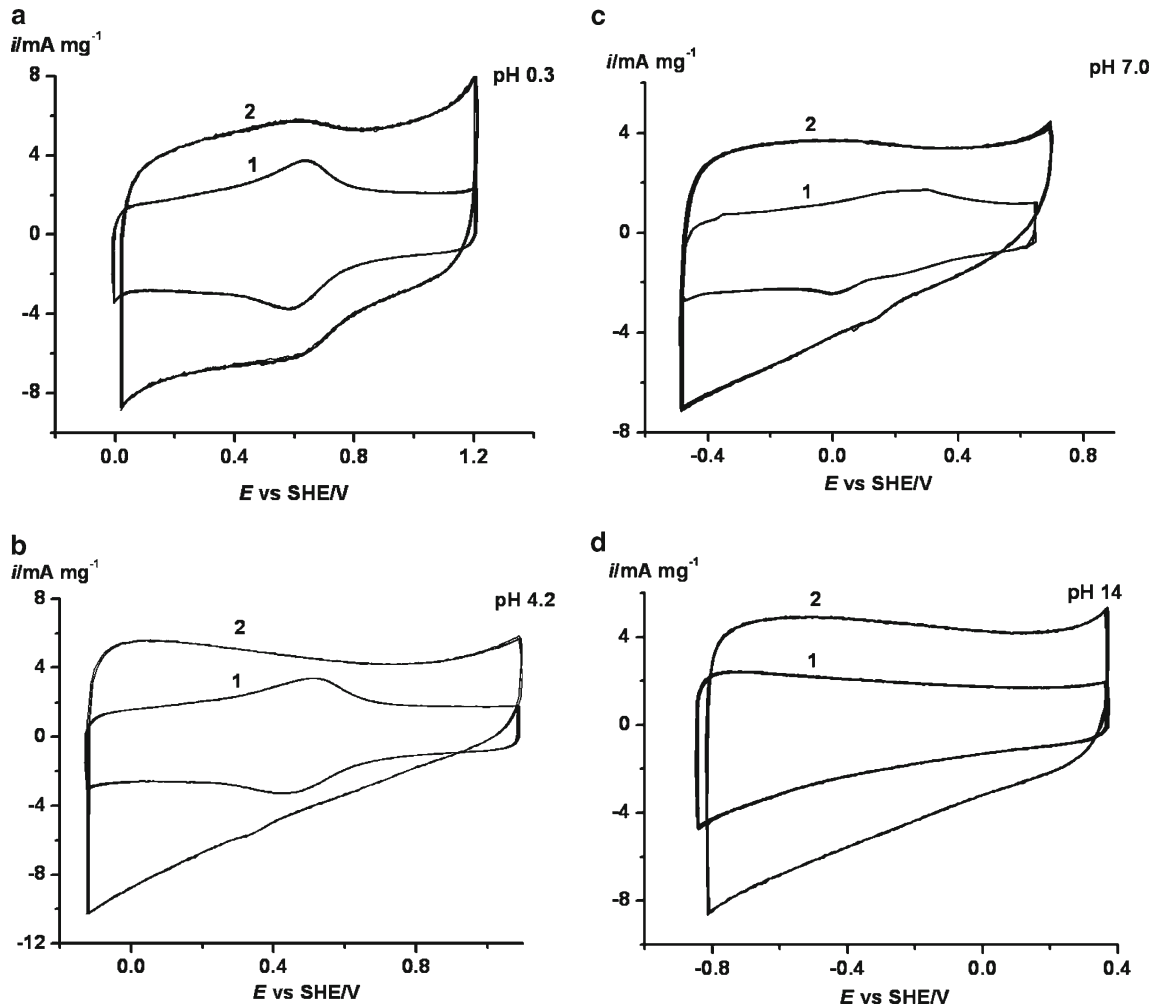

Fig. 7 CVA for XC72R (*1*) and MXC72R (*2*) in the solutions with different pH values: 0.3 (**a**), 4.2 (**b**), 7.0 (**c**), and 14 (**d**)

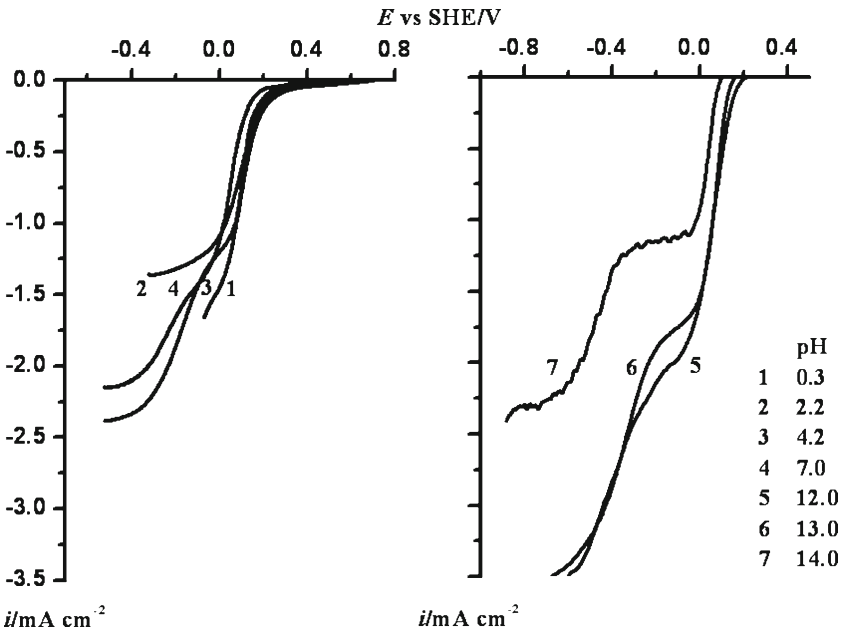

Fig. 8 Polarization curves for the ORR on carbon black XC72R in solutions with various pH values; 0.002 V s^{-1}; 635 rpm

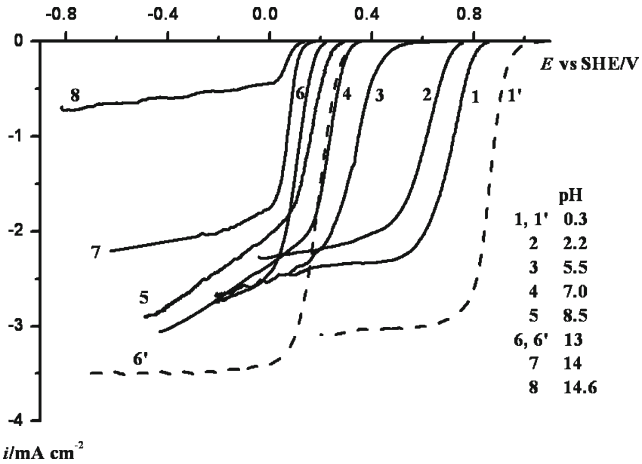

Fig. 9 Polarization curves for the ORR on MXC72R catalyst (*1*–*8*) and Pt/C (*1′*, *6′*) in solutions with various pH values; 0.002 V s^{-1}; 635 rpm

accounts for the fact that the average electron number in the region of limiting current exceeds 3 (Table 2).

pH influence on half-wave potential

At half-wave potential ($E_{1/2}$), pH dependence characterizes the kinetics of the ORR at identical transport conditions (equal thickness of active layer) at RDE. As seen from Figs. 8 and 10, $E_{1/2}$ values for XC72R in acid and neutral solutions does not depend on pH. In contrast to this, polarization curves for MXC72R are negatively shifted for ~−0.060 V per pH unit (Figs. 9 and 10). This fact reminds the behavior of disperse platinum catalyst on carbon support; however, the value of $E_{1/2}$ for monoplatinum catalyst is substantially more positive (ca. 0.2 V) than for MXC72R. In alkaline solution with pH>12, the value of $\frac{dE_{1/2}}{dpH}$ for XC72R and MXC72R is changed and amounts to −0.015 to 0.020 (in comparison to $\frac{dE_{1/2}}{dpH}$ ~−0.060 V for platinum). Polarization curves presented in Fig. 8 show that remarkable reduction of oxygen at turbostratic carbon starts at $E<0.2$ V. Thus, the ORR at MXC72R in solutions with pH ≤7 at potential $E>0.2$ V (Fig. 9) takes place at the utmost degree at AC generated during CoTMPP pyrolysis. At higher cathode polarization, the process can also be performed at the carbon support. However, this current does not give notable contribution to the overall O_2 reduction current.

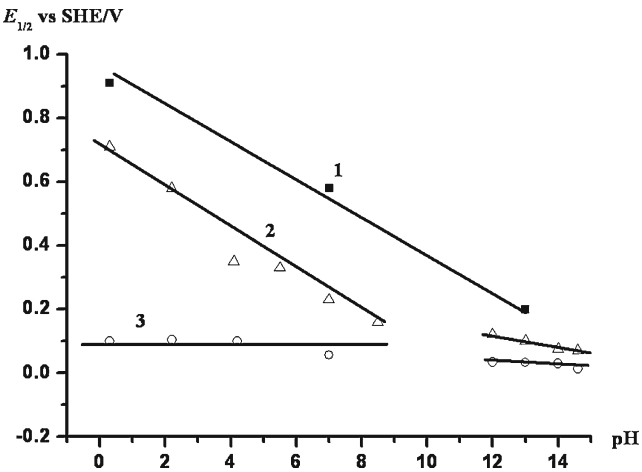

Fig. 10 pH dependence of half-wave potential for the ORR on the following materials: 40Pt/C (*1*), MXC72R (*2*), XC72R (*3*)

pH and Tafel plots

Figure 11a,b show mass transport-corrected Tafel plots for XC72R and MXC72R. Tafel plots for XC72R (Fig. 11a) have close slope values for the solutions with pH 0.3 (curve 1) and 7.0 (curve 2). For pH 0.3, the slope equals −0.120 to −0.130 V. With pH increased to 7.0, the value is a little changed (to −0.100 V). Polarization curves obtained in the alkaline solution (pH 13.0) have lower slope values as seen from curve 3. First, the slope, ~−0.030 V per decade, is observed in the potential interval between 0.07 and 0.12 V. When more

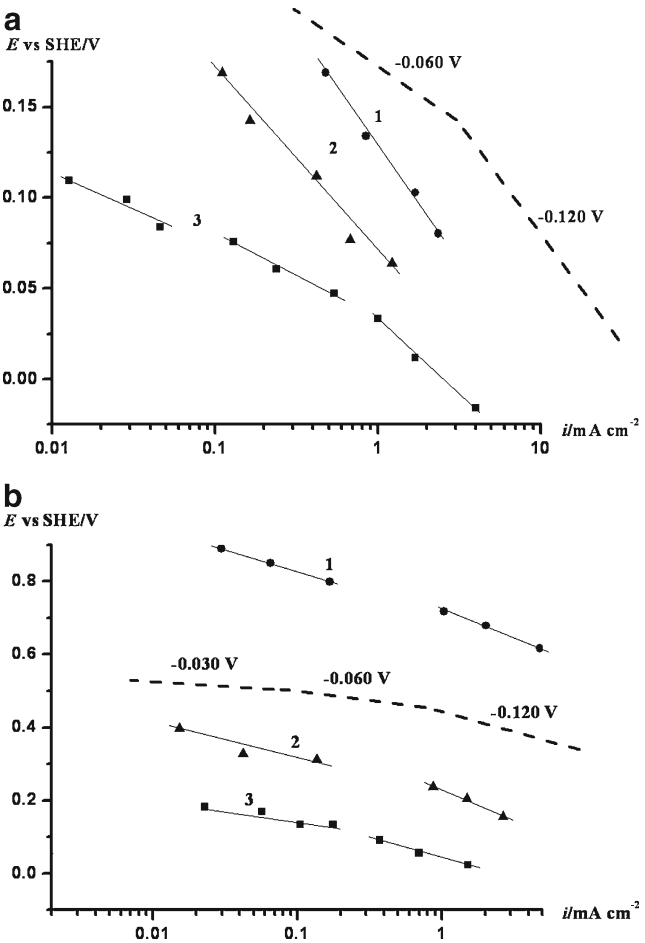

Fig. 11 Mass transport corrected Tafel plots for the ORR on XC72R (**a**) and MXC72R (**b**) at pH 0.3 (*1*), 7.0 (*2*), and 13.0 (*3*). 0.002 V s^{-1}, O_2

cathodic potential is applied, the slope is smoothly changed first to −0.040 to −0.060 V and then to −0.080 to −0.090 V.

As shown in Fig. 11b, curve 1 for MXC72R at pH 0.3 at low polarization, the slope value composes −0.060 V; at higher polarization, the slope is changed to −0.130 V. When passing to neutral solutions (curve 2), the region with a slope of −0.060 V is extended. At pH 13 (curve 3), the slope of −0.030 V is not observed at all in contrast to XC72R; the region with a slope of about −0.060 V per decade is expressed more clearly.

It ought to be noted that the evaluation of the slope values for different parts of the Tafel plots is a fairly conventional procedure. Nevertheless, these data should be used and explained on discussion of the ORR mechanism.

Table 3 Kinetic constants of the ORR partial reactions for XC72R (0.1 mg cm^{-2}) and MXC72R (0.15 mg cm^{-2}) in 0.1 M H_2SO_4

E, V	$k_1 \cdot 10^2$	$k_2 \cdot 10^2$	k_1/k_2	$(k_3+k_4) \cdot 10^2$
XC72R				
0.05	0.036	0.96	0.0325	3.70
0.00	0.060	1.75	0.035	1.88
−0.05	0.100	4.20	0.025	1.55
−0.10	0.150	6.00	0.026	0.23
MXC72R				
0.6	1.1	0.46	2.38	0.056
0.5	3.0	1.34	2.22	0.130
0.4	5.9	2.77	2.15	0.140

The pathways of the ORR at different pH

Figure 12 presents polarization curves of the ORR in 0.1 M H_2SO_4 at disk electrode and oxidation current of hydrogen peroxide at ring electrode. It is evident that the catalytic activity of MXC72R is incomparably higher than that of XC72R. Apparently, in the potential interval between 0.9 and 0.4 V, the CoTMPP pyrolysis products are responsible for the ORR catalysis, not the carbon support. Herewith, the current value at ring electrode is increased with cathode polarization. As seen from Table 3, k_1/k_2 ratio at XC72R is close to zero and the direct reaction to water is practically absent. For MXC72R, k_1 and k_2 are within the same order of magnitude, the former being somewhat higher to give the ratio $k_1/k_2>2$ and the portion of direct reaction arrives at 70 %. At platinum in similar conditions, the contribution of direct reaction to water is close to 95 % [53].

XC72R and MXC72R showed opposite dependencies of the constant sum (k_3+k_4) on the potential. The decrease of the constant sum for XC72R likely witness the decrease in the rate of hydrogen peroxide catalytic decomposition (k_4). In the case of MXC72R, the sum increase mainly corresponds to the growth of electrochemical H_2O_2 reduction rate (k_3).

The measurements with RRDE for XC72R and MXC72R were also performed in neutral (pH 7) and alkaline (pH 12) solutions (Fig. 13a, b). These data confirm once more that in

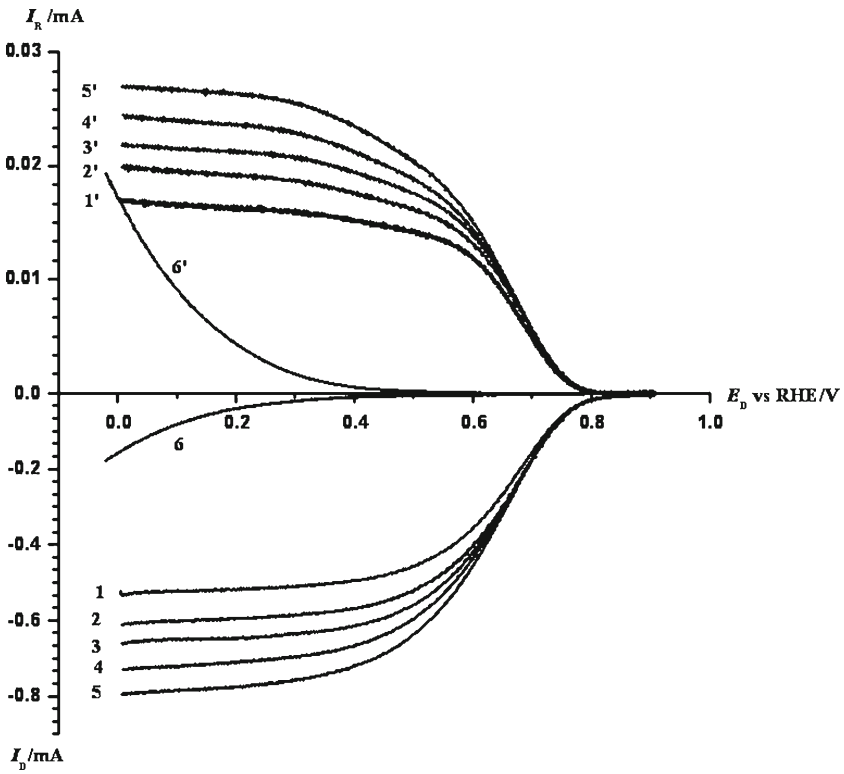

Fig. 12 Polarization curves for the ORR on a thin-film RRDE with MXC72R (*1*–*5*) and simultaneously recorded ring currents for a ring potential of E_R=1.23 V (*1′*–*5′*) at *m*, rpm: 700 (*1*), 900 (*2*), 1,100 (*3*), 1,300 (*4*), 1,500, (*5*) 0.1 M H_2SO_4, 25 °C, 0.005 V s^{-1}. For comparison the data for the ORR on XC72R at 700 rpm are presented (*6*, *6′*)

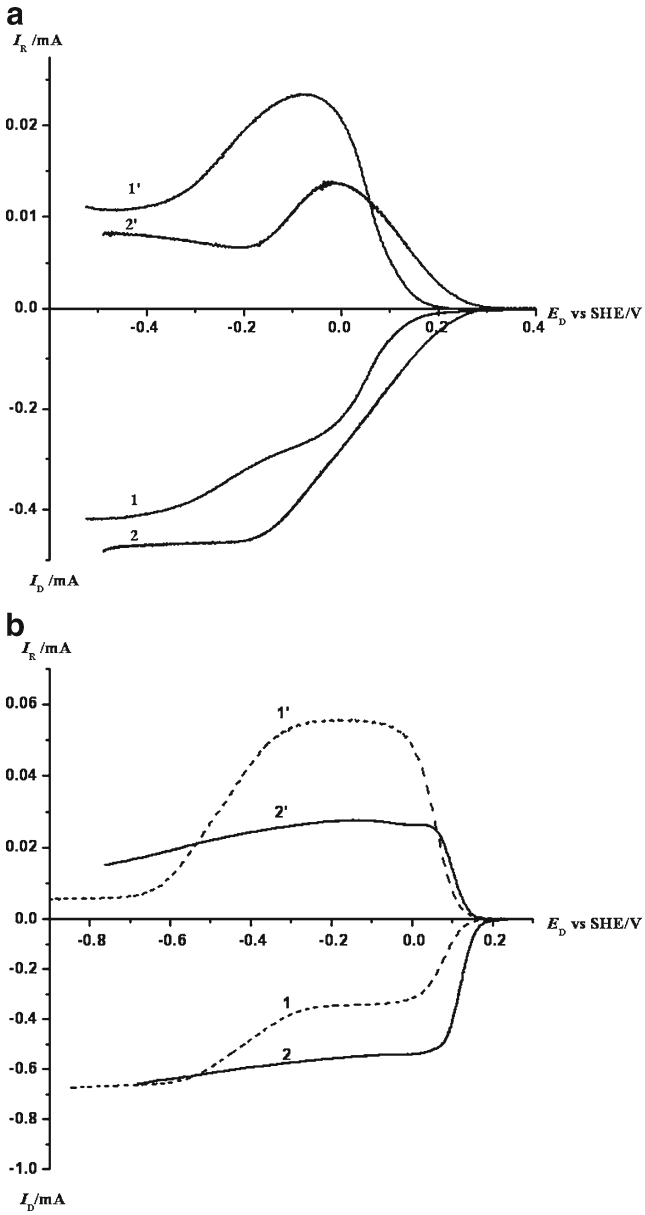

Fig. 13 Polarization curves for the ORR on a thin-film RRDE with XC72R (*1*) and MXC72R (*2*) and simultaneously recorded ring currents for a ring potential of E_R=1.23 V (*1′*, *2′*) in solutions with pH 7.0 (**a**) and 12.0 (**b**). 700 rpm. 0.1 M H_2SO_4, 25 °C, 0.005 V s^{-1}

the polarization region, between the steady-state potential E_s (presented in Table 2) and ca. 0.2 V, the ORR proceeds at AC

Table 4 Kinetic parameters of the ORR for MXC72R (0.15 mg cm^{-2}) catalyst. 0.1 M KOH, 25 °C

E, V	$k_1 \cdot 10^2$, cm/s	$k_2 \cdot 10^2$, cm/s	k_1/k_2	$(k_3+c_4) \cdot 10^2$, cm/s
0.13	1.24	1.32	0.94	0.43
0.08	2.40	2.52	0.95	–
0.03	3.00	3.30	0.91	0.43
−0.02	2.80	3.00	0.93	–

formed in CoTMPP pyrolysis process. From the data in Table 4, a conclusion could be made that the ORR at MXC72R in alkaline solution proceeds simultaneously and equally via as the direct reaction with OH^- ion formation and two-electron reaction with production of HO_2^-. Meanwhile, the certain part of HO_2^- produced is subjected to the catalytic decomposition or electrochemical reduction. The cathode polarization leads to the increase of k_1 and k_2; moreover, k_1/k_2 ratio is unaffected and it is twofold smaller in comparison to acid electrolyte (Fig. 14).

Thus, the ORR selectivity to direct water (or OH^-) formation for XC72R and MXC72R in acid and alkaline solutions was analyzed in the current paper. According to the data obtained and the data published on Pt [76–79], the materials could range in the following decreasing selectivity order for the four-electron reduction of oxygen:

Pt > MXC72R > XC72R.

The analysis of literature data permits concluding that adsorption energy of molecular oxygen is decreased in the same sequence of materials. According to calculations [80], the adsorption heat of the molecular oxygen at platinum (~2.68 eV) is considerably higher in comparison to carbon. The research on oxygen dissociation on carbon nanotubes (CNT) [81] showed that binding energy of oxygen with CNT composes ~0.25 eV and oxygen molecule dissociation energy is ~2 eV. The introduction of nitrogen atoms into CNT resulted in lowering of the dissociation energy to ~0.68 eV. Thus, we believe that MXC72R occupy intermediate position between platinum and turbostratic carbon in accordance with the oxygen binding energy value.

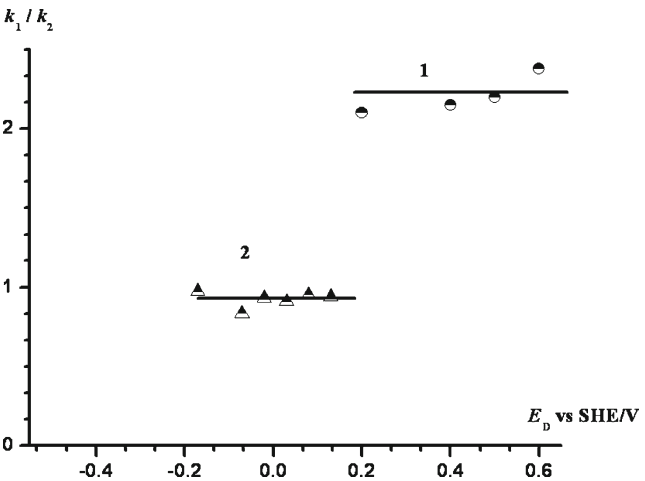

Fig. 14 The constant ratio k_1/k_2 for MXC72R at various potentials in solutions with pH 0.7 (*1*) and 13.0 (*2*)

Mechanism of the ORR

To discuss the ORR mechanism at such a variety of catalytic systems as turbostratic carbon, nitrogen-doped carbon, and platinum, besides the experimental data, it is necessary to take account of the thermodynamics of the most important oxygen reactions [82] and quantum chemical calculations (the number of which is permanently increased).

The most widespread approach [59, 83, 84] of the ORR mechanism described is the suggestion that the rate-determining stage (RDS) is the first electron transfer for all materials under study:

$$O_2 + \bar{e} \rightarrow O_2^- \quad (5)$$

standard equilibrium potential of which does not depend on pH and equals to $E^{\circ}{}_{o_2/o_2-} = -0.31\text{V}$ [63]. By contrast, the equilibrium potentials of four- and two-electron reactions of the *ORR*, $\text{E}^0_{\text{O}_2/\text{H}_2\text{O}} = 1.23\,\text{V}$ and $E^0_{\text{O}_2/\text{H}_2\text{O}_2} = 0.682\,\text{V}$, depend on pH with the coefficient of $\frac{dE}{dph} = -0.059\text{V}$ with the exception of the alkaline solutions where in the case of the two-electron reaction, the slope value changed to −0.030 V (Fig. 15). That is why, as was noticed in [82], overvoltage of the ORR in relation to the RDS (1) is gradually lowered at passing from acid solutions to alkaline. This was proved experimentally in Fig. 10 and follows from the calculations [85] according to which the activation energy of electron transfer to $O_{2(\text{ads})}$ at platinum in alkali does not exceed 0.1 eV.

One of the key factors governing kinetics, mechanism, and pathways of the ORR is the adsorption energy of the oxygen molecule on the catalyst surface. The values of adsorption energy are not experimentally determined for electrolyte solutions. For their estimation, theoretical calculations could be used. As mentioned above, the binding energy of the oxygen molecule with graphite-like materials is low. Meanwhile, very insignificant (~0.01 eV) electron transfer from carbon to oxygen molecule is expected [86]. Under these conditions, high overvoltage of the ORR is observed and no O–O bond disruption occurs. The mechanism is described by the following sequence of reactions for carbon materials:

$$M + O_2 \rightarrow MO_2 \quad (6)$$

$$MO_2 + \bar{e} \xrightarrow{\text{RDS}} MO_2^- \quad (7)$$

$$MO_2^- + H_2O + \bar{e} \rightarrow M + HO_2^- + OH^- \quad (8)$$

with RDS (7) and subsequent reduction to hydrogen peroxide. This explains the value of $\frac{dE_{1/2}}{dpH} \sim 0\,\text{V}$ in a broad pH interval and the ORR proceeds only through two-electron pathway.

The experimental values of the Tafel slope about −0.100 to −0.120 V support the fact that the RDS is the first electron transfer under conditions of oxygen adsorption energy independence on potential (Langmuir isotherm). In alkaline solutions, the slope value of ~−0.030 V observed in the region of low polarization corresponds to O_2/HO_2^- equilibrium and is explained by concentration polarization on HO_2^- withdrawal. The change of the slope to −0.050 and later to −0.090 V with polarization could be explained by OH^- ion adsorption blocking the places for oxygen molecule adsorption. As a result, the energy of oxygen molecule adsorption becomes dependent on potential and the reaction is governed by Temkin isotherm even at low surface coverage by $O_{2(\text{адс})}$ species. There is another opinion [87] according to which the second electron transfer could also be the RDS under the conditions of low activation energy of the first electron transfer in alkaline solution.

As follows from the data presented, the ORR regularities (Tafel slopes in different solutions, pH dependence of $E_{1/2}$) at MXC72R differ significantly from these of turbostratic carbon, and MXC72R resembles platinum for many kinetic parameters, namely,

- $\frac{dE_{1/2}}{dpH} \sim -0.06\text{V}$ in a broad range of pH
- two Tafel slopes of ~−0.060 and ~−0.120 V per decade in acid and neutral solutions
- the only Tafel slope of ~−0.060 V per decade in alkaline solutions and the absence of the slope of ~−0.030 V

Similar data for the ORR at platinum were repeatedly described [72, 88, 89] and generalized in [59, 83, 84]. Meanwhile, the ORR proceeds as through intermediate formation of H_2O_2 (HO_2^-) and direct reaction to H_2O (OH^-) in both acid and alkaline solutions

The quantum chemical analysis in [90] has shown that the proton participation in the RDS of the first electron transfer (7) in acid solutions is necessary for lowering its overvoltage. The

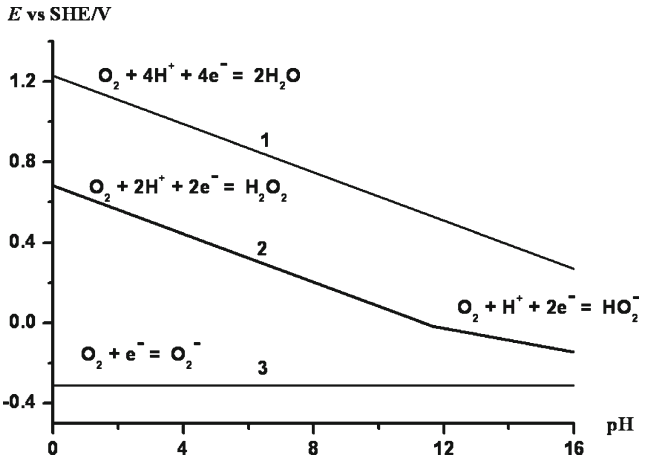

Fig. 15 Model diagram $E^0 = f(\text{pH})$ for various reactions of the ORR

protonation decreases the activation barrier of electron transfer from 0.74 eV for O_2 to 0.06 eV for OOH. For platinum, the oxygen binding energy with the surface is high and, consequently, there is a significant transfer of electron to the adsorbed O_2 molecule and the formation of binding with electrolyte proton. This facilitates the first electron transfer, weakening the O–O binding and providing its disruption. Proton participation in the RDS results in the decrease of the overvoltage in comparison to carbon and allows achieving high selectivity in respect to water formation.

In this case, for platinum, the ORR is described by the following stages:

$$M + O_2 + H^+ \overset{RDS}{\rightarrow} MO_2 --- H_\nu^+ \quad (9)$$

$$MO_2 --- H_\nu^+ + \bar{e} \rightarrow MO_2H \quad (10)$$

$$MO_2H + \bar{e} \rightarrow MO + OH^- \quad (11)$$

with the RDS (9) where ν is the extent of proton participation in protonation reaction.

Evidently, nitrogen-containing carbon materials occupy an intermediate position between low-active turbostratic carbon and highly active platinum catalysts in accord with their adsorption properties in respect to O_2 and their reduction efficiency.

Due to the free electrons on pyridine and quaternary atoms of nitrogen, the strong O_2 adsorption with partial electron transfer and the protonation of the oxygen molecule become possible. In acid and neutral solutions, the ORR proceeds via the stages (9)–(11). In alkaline solutions where water serves as the proton source, the mechanism described by the stages (6)–(8) prevails. Hindrance of O_2 molecule protonation in alkaline solutions results in lowering of the ORR selectivity as in the case of platinum.

Generalized equation describing both mechanisms is

$$i = k\, p_{O_2}\, c_{H^+}^{\gamma} \exp\left(-\frac{\alpha FE}{RT}\right) \exp(\pm \Sigma \gamma f \theta_i) \quad (12)$$

which includes proton concentration in fractional degree ν. The last factor $\exp(\pm\Sigma\gamma f\theta_i)$ makes allowance into the dependence of adsorbed oxygen energy on surface coverage by foreign blocking species. The effect of blocking species is pronounced at Pt(111) [91–93] especially strongly at clear perception of the nature of these foreign-blocking species. In the case of carbon and other low-active catalysts, the nature of active centers for the ORR is not clear; moreover, the character of their blocking is not known. In this case, the last factor could be considered as the change of density of AC and even their nature with electrode polarization. This equation will be improved in the process of obtaining new experimental data. More complicated anamorphosis of this equation is represented in [94]. Analogous approach was used in [91, 95].

It is not difficult to see that Eq. (12) describes the main experimental data for electrode materials under study. At $\nu \sim 0.5, \frac{dE_{1/2}}{d\lg i} \sim -2.3\frac{RT}{F}$, the Tafel plot slope changing from $\sim -2.3\frac{RT}{F}$ to $-2 \times 2.3\frac{RT}{F}$ is due to O_2 adsorption energy changing from Temkin isotherm conditions to Langmuir isotherm conditions. At $\nu \sim 0$, the dependence on pH is absent.

The described approach is rather formal as analysis of kinetic parameters is performed phenomenologically. The quantitative description of O_2 adsorption energy influence and its protonation on the rate and selectivity of the ORR on different materials could be found in the context of quantum chemical investigations.

In spite of indicated limitations, the approach developed in the current paper involving the analysis of the ORR rate and selectivity dependence on pH permits evaluation of the efficiency of various precious metal-free catalytic systems in comparison to platinum. Unlike the majority of papers studying the ORR kinetics and its mechanism for the only material in a narrow pH range, the advantage of the approach used here is that a series of catalysts was electrochemically characterized in a wide pH interval.

Conclusion

The resemblance of the key kinetic parameters of the ORR for platinum catalysts and modified carbon black in pH range of 0.3–9.0 is the evidence by the similarity of the ORR mechanism. At both catalysts, the ORR proceeds with the same rate-determining stage of the first electron transfer and protonation of the adsorbed oxygen molecule (9). The protonation facilitates the proceeding of the stage (7) weakening of O–O bonding and favors the enhancement of the ORR selectivity in respect to four-electron route.

The possibility of such a mechanism depends largely on the character of oxygen molecule adsorption (coordination). Only rather strong adsorption of oxygen molecule, accompanied by significant localization of negative charge on it, creates the conditions for protonation. The lower value of oxygen molecule adsorption energy at MXC72R in comparison to platinum is responsible for half-wave potential shift to negative side. Meanwhile, the fraction of direct reaction to water in acid solution composes 70 versus 95 % for platinum electrode. In alkaline solutions, oxygen molecule adsorbs at MXC72R less strong as compared to platinum and its protonation is hindered. It is this reason that the first electron transfer reaction, the rate of which does not depend on pH, becomes the RDS of the ORR. In neutral solutions, water molecules serve as the source of protons. The change in the Tafel slope when the pH dependence is constant is due to surface coverage change by blocking species.

Thus, the performed study permitted to establish the reasons of lower electrocatalytical activity of catalysts not containing platinum group metals in comparison to platinum and to trace the ways on how it is overcome. Meanwhile, the important approach is the testing of electrochemical parameters of new catalytic systems in a broad pH interval.

Acknowledgments This work was supported by the Russian Foundation for Basic Research grant no 13-03-00317a.

References

1. Bagotsky VS (2006) Fundamentals of electrochemistry. Wiley, New York
2. Bagotsky VS (2009) Fuel cells: problems and solutions. Wiley, New York
3. Bagotsky VS, Jablokova IE (1953) Russian J Phys Chem 27:1663–1667
4. Bagotsky VS, Filinovskii VJ, Shumilova NA (1968) Soviet Electrochem 4:1129–1133
5. Bagotsky VS, Tarasevich MR, Filinovskii VJ (1969) Soviet Electrochem 5:1158–1161
6. Bagotsky VS, Tarasevich MR, Filinovskii VJ (1972) Soviet Electrochem 8:81–84
7. Bagotsky VS, Tarasevich MR, Radyushkina KA, Levina OA, Andrusyova SI (1978) J Power Sources 2:233–240
8. Kinoshita K (1988) Carbon—electrochemical and physicochemical properties, vol 1. Wiley, New York
9. Kruusenberg I, Leis J, Arulepp M, Tammeveski K (2010) J Solid State Electrochem 14:1269–1277
10. Kruusenberg I, Matisen L, Shah Q, Kannan AM, Tammeveski K (2012) Int J Hydrogen Energy 37:4406–4412
11. Kruusenberg I, Alexeyeva N, Tammeveski K (2009) Carbon 47:651–658
12. Zimmermann G, Schonborn M, Magenau H, Jahnke H, Becker B (1976) Patent USA 3:930,884
13. Jahnke H, Schonborn M, Zimmermann G (1976) Top Curr Chem 61:131–138
14. Scherson D, Tanaka A, Gupta S, Tryk D, Fierro C, Holze R, Yeager E, Latimer R (1986) Electrochim Acta 31:1247–1258
15. Iliev I, Gamburzev S, Kaisheva A, Fuhrmann A, Wiesener K (1984) J Power Sources 13:217–222
16. Wiesener K (1986) Electrochim Acta 31:1073–1078
17. Gouerec P, Bilou A, Contamin O, Scarbeck G, Savy M, Barbe J, Guilard R (1995) J Electroanal Chem 398:67–75
18. Claude E, Addou T, Latour J-M, Aldebert P (1998) J Appl Electrochem 28:57–64
19. Tyurin SS, Radyushkina KA, Levina OA, Tarasevich MR (2001) Russian J Electrochem 37:843–847
20. Zagal J (2003) In: Vielstich W, Lamm A, Gasteiger H (eds) Handbook of fuel cells. Fundamental, technology and applications. Wiley, New York
21. Mocchi C, Trasatti S (2003) J Mol Catal A: Chem 204–205:713–720
22. Lefevre M, Dodelet J.-P, Bertrand P (2005) J Phys Chem B 10916718–16724
23. Herrmann I, Bruser V, Fiechter S, Kersten H, Bogdanoff P (2005) J Electrochem Soc 152:A2179–A2185
24. Dodelet J-P (2006) In: Zagal J, Bedioui F, Dodelet J-P (eds) N_4-macrocyclic metal complexes. Springer, Berlin
25. Zagal J (2006) In: Zagal J, Bedioui F, Dodelet J-P (eds) N_4-macrocyclic metal complexes. Springer, Berlin
26. Artyushkova K, Pylypenko S, Olson T, Fulghum J, Atanassov P (2008) Langmuir 24:9082–9088
27. Tarasevich MR, Radyushkina KA (1982) Catalysis and electrocatalysis by metalloporphyrins. Nauka, Moskwa
28. Zagal JH, Bedioui F, Dodelet J-P (eds) (2006) N_4-macrocyclic metal complexes. Springer, Berlin
29. Jaouen F, Herranz J, Lefevre M, Dodelet J-P, Kramm UI, Herrmann I, Bogdanoff P, Maruyama J, Nagaoka T, Garsuch A, Dahn JR, Olson T, Pylypenko S, Atanassov P, Ustinov EA (2009) ACS Appl Mater Interfaces 1:1623–1639
30. Tarasevich MR, Radyushkina KA, Zhutaeva GV (2004) Russian J Electrochem 40:1174–1187
31. Pylypenko S, Mukherjee S, Olson TS, Atanassov P (2008) Electrochim Acta 53:7875–7883
32. Liu G, Li X, Ganesan P, Popov BN (2010) Electrochim Acta 55:2853–2858
33. Liu G, Li X, Lee J-W, Popov BN (2011) Catal Sci Technol 1:207–217
34. Maldonado S, Stevenson KJ (2004) J Phys Chem B 108:11375–11383
35. Maldonado S, Morin S, Stevenson KJ (2006) Carbon 44:1429–1437
36. Wiggins-Camacho JD, Stevenson KJ (2009) J Phys Chem C 113:19082–19090
37. Wiggins-Camacho JD, Stevenson KJ (2011) J Phys Chem C 115:20002–20010
38. Kruusenberg I, Matisen L, Tammeveski K (2013) Int J Electrochem Sci 8:1057–1066
39. Tarasevich MR, Radiyschkina KA, Androuseva SI (1977) Bioelectrochemistry 4:18–29
40. McIntyre NS, Cook MG (1975) Anal Chem 47:2208–2213
41. Tarasevich MR, Bogdanovskaya VA, Kazanskii LP, Lozovaya OV, Mazin PV (2010) Protect Metals Phys Chem Surf 46:39–48
42. Schmidt TJ, Gasteiger HA (2003) In: Vielstich W, Gasteiger HA, Lamm A (eds) Handbook of fuel cells—fundamentals, technology and applications. Wiley, New York
43. Zhutaeva GV, Tarasevich MR (2010) Protect Metals Phys Chem Surf 46:215–221
44. Bonakdarpour A, Lefevre M, Yang R, Jaouen F, Dahn T, Dodelet J-P, Dahn JR (2008) Electrochem Solid-State Lett 11:B105–B108
45. Frumkin AN, Tedoradze GA (1858) Dokl Chem 118:530–533
46. Frumkin AN, Aikazyan EA (1959) Izv Acad Sci USSR. chem sci 2:202–213
47. Levich VG (1962) Physicochemical hydrodynamics. Prentice Hall, New York
48. Albery WJ, Bruckenstein S (1966) Trans Faraday Soc 62:1920–1931
49. Tarasevich MR, Khrushcheva EI, Filinovskii VJ (1987) Rotating ring-disk electrode. Nauka, Moskwa
50. Biddinger EJ, von Deak D, Singh D, Marsh H, Tan B, Knapke DS, Ozkan US (2011) J Electrochem Soc 158:B402–B409
51. Tarasevich MR (1969) Soviet Electrochem 5:663–665
52. Wroblowa HS, Pan Y-C, Razumney G (1976) J Electroanal Chem 69:195–201
53. Paulus UA, Schmidt TJ, Gasteiger HA, Behm RJ (2001) J Electroanal Chem 495:134–145
54. Chen S, Kucernak A (2004) J Phys Chem B 108:3262–3276
55. Stewart KJ, Gewirth AA (2007) Langmuir 23:9911–9918
56. Coutanceau C, Hourch AE, Crouigneau P, Leger J-M, Lamy C (1995) Electrochim Acta 40:2739–2748
57. Gubbins KE, Walker RD (1965) J Electrochem Soc 112:469–471
58. Nekrasov LN (1966) Soviet Electrochem 2:419–423
59. Tarasevich MR, Sadkowski A, Yeager E (1983) In: Conway BE, Bockris JO'M, Yeager E, Khan SUM, White RE (eds) Comprehensive treatise of electrochemistry. Plenum Press, New York
60. Strbac S (2011) Electrochim Acta 56:1597–1604
61. Strbac A, Adžić RR (1996) Electrochim Acta 41:2903–2908
62. Liu H, Zhang L, Zhang J, Ghosh D, Jung J, Downing BW, Whittermore E (2006) J Power Sources 161:743–752
63. Yang H-H, McCreery L (2000) J Electrochem Soc 147:3420–3428

64. Shao M, Liu P, Adzic RR (2006) J Am Chem Soc 128:7408–7409
65. Maldonado S, Stevenson KJ (2005) J Phys Chem B 109:4707–4716
66. Shao MN, Adzic RR (2005) J Phys Chem B 109 (2005) 16563–16566
67. Bonakdarpour A, Dahn TR, Atanasoski RT, Debe MK, Dahn JR (2008) Electrochem Solid-State Lett 11:B208–B211
68. Inaba M, Yamada H, Tokunaga J, Tasaka A (2004) Electrochem Solid-State Lett 7:A474–A476
69. Bonakdarpour A, Delacote C, Yang R, Wieckowski A, Dahn JR (2008) Electrochem Commun 10:611–615
70. Feng Y, He T, Alonso-Vante N (2009) Electrochim Acta 54:5252–5256
71. Tsivadze AJ, Tarasevich MR, Kuzov AV, Kuznetsova LN, Lozovaja OV, Davydova ES (2012) Dokl Chem 442(2012):45–48
72. Ross PN (2003) In: Vielstich W, Lamm A, Gasteiger HA (eds) Handbook of fuel cells. Fundamentals, technology and applications. Wiley, New York
73. Tarasevich MR, Korchagin OV (2013) Rus J Electrochem 49:600–618
74. Zoltowski P (1976/1977) J Power Sources 1:285–298
75. Andreas HA, Conway BE (2006) Electrochim Acta 51:6510–6520
76. Hsuen K-L, Chin D-T, Srinivasan S (1983) J Electroanalyt Chem 153:79
77. Schmidt TJ, Paulus UA, Gasteiger HA, Behm RJ (2001) J Electroanal Chem 508:41–47
78. Gasteiger HA, Kocha SS, Sompalli B, Wagner FT (2005) Appl Catal B Environ 56:9–35
79. Tarasevich MR, Mazin PV, Kapustina NA (2011) Russian J Electrochem 47:923–932
80. Hammer B, Norskov JK (2000) Adv in Catal 45:71–129
81. Shan B, Cho K (2010) Chem Phys Lett 492:131–136
82. Blizanac BP, Ross RN, Markovic NM (2007) Electrochim Acta 52: 2264–2271
83. Sepa DB, Vojnovich MV, Damjanovic A (1981) Electrochim Acta 26:781–793
84. Adzic R (1998) In: Lipkowski J, Ross RN (eds) Electrocatalysis. Wiley, New York
85. Anderson AB, Zhang T (2007) Electrochim Acta 53:982–989
86. Sorescu DC, Jordan KD, Avouris P (2001) J Phys Chem B 105: 11227–11232
87. Appleby AJ, Marie J (1979) Electrochim Acta 24:195–202
88. Damjanovic A, Damjanovic A (1969) In: Bockris JO'M, Conway BE, Bockris JO'M, Conway BE (eds) Modern aspects of electrochemistry. Plenum Press, New York
89. Damjanovic A (1992) In: Murphy OJ, Srinivasan S, Conway BE (eds) Electrochemistry in transition. Plenum Press, New York
90. Sidik RA, Anderson AB (2002) J Electroanal Chem 528:69–79
91. Markovich NM, Gasteiger HA, Grgur BN, Ross PN (1999) J Electroanal Chem 476:157–163
92. Wang JX, Markovic NM, Adzic RR (2004) J Phys Chem B 108: 4127–4133
93. Wang JX, Zhang J, Adzic RR (2007) J Phys Chem A 111:12702–12710
94. Tarasevich MR (1981) Soviet Electrochem 17:988–992
95. Subramanian NP, Greszler TA, Zhang J, Gu W, Makharia R (2012) J Electrochem Soc 159:B531–B540